# Supporting Information: Polymersomes with Asymmetric Membranes and Self-assembled Superstructures Using Pentablock Quintopolymers Resolved by Electron Tomography

J. S. Haataja[a], N. Houbenov[*a], V. Aseyev[b], P. Fragouli[c], H. Iatrou[c], R. Sougrat[d], N. Hadjichristidis[*d] and O. Ikkala[*a]

## 1 Materials

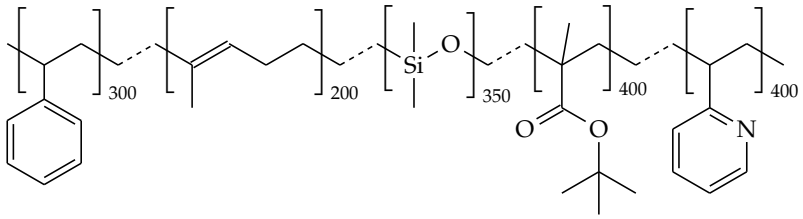


**Fig**. S1: The pentablock quintopolymer; PS-*block*-PI-*block*-PDMS-*block*-PtBMA-*block*-P2VP. The respective (rounded) degrees of polymerization are shown in subscripts.

The synthesis of pentablock quintopolymer, polystyrene -*block*-poly(1,4-isoprene) -*block*-poly(dimethyl siloxane) -*block*-poly(*tert*-butyl methacrylate) -*block*-poly(2-vinyl pyridine), i.e., PS-*b*-PI-*b*-PDMS-*b*-PtBMA-*b*-P2VP) (see Fig. S1), with respective block lengths of 32.4, 13.1, 24.7, 50 and 41.7 kg/mol, using polymerization high vacuum techniques is reported in [1].

[a]. Department of Applied Physics, Aalto University, FI-00076, Aalto, Espoo, Finland.
E-mail: nikolay.houbenov@aalto.fi, olli.Ikkala@aalto.fi
[b]. Department of Chemistry, University of Helsinki
P.O.Box 55, FI-00014 Helsinki, Finland
[c]. Chemistry Department, University of Athens, Panepistimiopolis, Zografou, 15771, Athens, Greece.
[d]. King Abdullah University of Science and Technology (KAUST), Thuwal 23955-6900, Kingdom of Saudi Arabia.
E-mail: nikolaos.hadjichristidis@kaust.edu.sa.

Table S1: Physical properties for the polymer blocks.

| Block | $M_{w,\text{block}}$ | $M_{w,\text{repeat unit}}$ | DP | $\rho_a$ | $\rho_c$ | $V_{\text{Block}}$ | $\phi_{\text{frac.}}$ | $T_g$ | Refs. |
|---|---|---|---|---|---|---|---|---|---|
| | [kg/mol] | [g/mol] | | [g/cm$^3$] | [g/cm$^3$] | [cm$^3$/mol] | [%] | [°C] | |
| PS | 32.40 | 104 | 311 | 1.05 | 1.10 | 30 857 | 20 | 100 | [2, p. 922].[3, p. 443] |
| PI | 13.10 | 68 | 192 | 0.93 | | 14 086 | 9 | −58 | [3, p. 208. 444].[4] |
| PDMS | 24.70 | 74 | 333 | 0.97 | 1.07 | 23 084 | 15 | −123 | [3, p. 451].[2, p. 932-33] |
| PtBMA | 50.00 | 142 | 352 | 1.02 | | 48 924 | 32 | 114 | [2, p. 926] |
| P2VP | 41.70 | 105 | 397 | 1.14 | | 36 579 | 24 | 104 | [5] |

## 2 Solubility and miscibility of polymer blocks

Quantitative evaluation of solubility of each polymer block can aid the determination of the composition of polymersomes. Unfortunately a theory that would accurately predict the solubility of arbitrary polymer in arbitrary solvent does not exist. We use the Hansen [2, p. 206] solubility parameter

$$\delta^2 = \delta_d^2 + \delta_p^2 + \delta_h^2.$$

which works moderately well in many cases, and is more accurate than the Hildebrand solubility approach. The $\delta_d, \delta_p$ and $\delta_h$ are the dispersive, polar and hydrogen bonding solubility parameters respectively. The solubility of a polymer $P$ in an organic solvent $S$ can then be estimated based on solubility parameter difference

$$\Delta\delta = \left[(\delta_{d,P} - \delta_{d,S})^2 + (\delta_{p,P} - \delta_{p,S})^2 + (\delta_{h,P} - \delta_{h,S})^2\right]^{\frac{1}{2}}. \tag{1}$$

For good solubility $\Delta\delta$ should be $\leq 5\,(\text{MJ/m}^3)^{3/2}$ [2, p. 219]. In Table S2 these differences are calculated for a selection of solvents.

Table S2: The Hansen solubility parameter difference between polymer blocks and solvents. The difference is computed based on averaged literature values. According to the theory, the smaller the difference, the more miscible the components are. The theory has its shortcomings as it for instance predicts the solubility of P2VP in acetone, when situation is empirically known to be the opposite [6–8].

| $\Delta\delta$ [(MJ/m$^3$)$^{3/2}$] | PS | PI | PDMS | PtBMA | P2VP | $\mu(\Delta\delta)$ | $\sum\Delta\delta$ |
|---|---|---|---|---|---|---|---|
| PS | 0.0 | 6.0 | 8.5 | 4.2 | 4.4 | 4.6 | 23.1 |
| PI | 6.0 | 0.0 | 3.9 | 6.4 | 3.8 | 4.0 | 20.2 |
| PDMS | 8.5 | 3.9 | 0.0 | 7.3 | 7.6 | 5.5 | 27.4 |
| PtBMA | 4.2 | 6.4 | 7.3 | 0.0 | 6.7 | 4.9 | 24.6 |
| P2VP | 4.4 | 3.8 | 7.6 | 6.7 | 0.0 | 4.5 | 22.5 |
| Acetone | 5.3 | 9.1 | 10.6 | 3.3 | 8.2 | 7.3 | 36.5 |
| Chloroform | 5.1 | 3.7 | 3.7 | 4.7 | 5.9 | 4.6 | 23.1 |
| DCM | 2.9 | 5.4 | 6.6 | 1.8 | 5.6 | 4.5 | 22.3 |
| DMF | 9.2 | 14.2 | 15.2 | 8.2 | 13.2 | 12.0 | 59.9 |
| DMSO | 10.3 | 15.9 | 17.4 | 10.2 | 14.1 | 13.6 | 67.9 |
| Methanol | 18.8 | 22.4 | 21.4 | 16.5 | 22.8 | 20.4 | 101.9 |
| Ethanol | 15.4 | 18.4 | 17.2 | 12.9 | 19.2 | 16.6 | 83.2 |
| 1-Propanol | 13.4 | 15.8 | 14.4 | 10.7 | 17.0 | 14.3 | 71.3 |
| 2-Propanol | 12.5 | 14.7 | 13.1 | 9.8 | 16.0 | 13.2 | 66.2 |
| THF | 4.4 | 6.6 | 6.8 | 2.8 | 7.4 | 5.6 | 28.0 |
| Toluene | 7.0 | 1.8 | 3.7 | 7.8 | 4.9 | 5.0 | 25.1 |
| Water | 38.5 | 43.2 | 43.1 | 36.8 | 42.4 | 40.8 | 204.0 |

# 3 Methods

## 3.1 Sample preparation

Samples were prepared by dissolving PS-*b*-PI-*b*-PDMS-*b*-PtBMA-*b*-P2VP in acetone to obtain 1.0 % (w/w) solutions and left to mix overnight at 40 °C.

## 3.2 Transmission electron microscopy (TEM)

Transmission electron microscopy (TEM) imaging was carried out using a JEOL JEM 3200FSC field emission microscope operated at 300 kV in bright field mode with an Omega-type Zero-loss energy filter. The images were acquired with an ULTRASCAN™ 4000 CCD camera (GATAN) and with GATAN[1] DIGITALMICROGRAPH™ software while the specimen temperature was maintained at −187 °C. Additional TEM micrographs were images using 300 kV FEI Titan Krios in KAUST microscopy facilities.

Dry TEM samples were prepared by depositing 2–3 µl of sample solutions on holey carbon grids and then removing the excess with filter paper. For image alignment purposes, the TEM grids were dipped in 11-*mercapto-1-undecanol* ligand coated gold nanoparticle $d$ =3–10 nm solution before sample deposition [9]. $OsO_4$, $I_2$, $CH_3I$, and $RuO_4$ staining agents were introduced to the samples through vapour exposure. Typical staining times used were 120 min, 20 min, 20 min and 3 min respectively. Vitrified samples were prepared using FEI VITROBOT by placing 3–4 µl of sample solution on holey carbon grids under 5 and 100 % humidity, blotted with filter paper ca. 0.5–1.5 s for acetone and aqueous samples respectively and immediately plunged to −170 °C ethane/propane mixture and cryotransferred to the microscope.

## 3.3 Polymer phase identification using TEM

The assignment of block copolymeric microdomains in TEM micrographs is occasionally done by comparing the electron densities (=$\rho_{\text{mass}} \cdot n_e / M$) [10]. One could then expect P2VP to appear as the darkest microphase in comparison to PS, PtBMA, PI since $\rho_{e,\text{P2VP}} = 0.607 > \rho_{e,\text{PS}} = 0.565 > \rho_{e,\text{PtBMA}} = 0.561 > \rho_{e,\text{PI}} = 0.519$. However, PDMS involves a subtlety, as it is usually assigned as the darkest phase in block copolymer systems without staining, although it has relatively low electron density ($\rho_{e,\text{PDMS}} = 0.523$), [11] despite the presence of heavier silicon atoms. However, the relative highly brightness of polysilicates cannot be accounted by the mere presence of silicon e.g., poly(trimethyl silyl styrene) as convincingly shown by elemental mapping in TEM, to appear brighter than P2VP [5].

These apparent inconsistences have to do with the fact that, unlike X-rays, the contrast mechanism in TEM is mainly dependent on the scattering properties of atoms rather than mere electron densities [12], and thefore realiable interpretation of experimental results requires more subtle methods.

## 3.4 TEM simulations

To quantitatively estimate the image properties of the different polymer blocks to aid the interpretation of TEM images and tomographic reconstructions, we used multislice method for TEM simulations of amorphous specimens.

In the multislice method the specimen, described by the interaction potential[2] $\mathcal{V}^{\text{int}}(\mathbf{x}), \mathbf{x} = [x, y, z]$, is divided to thin slices of thickness $\Delta z \approx 1$ [12, Ch. 6.7]. The transmitted wave, at the top, $\mathbf{x}_{n+1} = [x, y, n\Delta z]$, of $n+1$:th slice, is then given by

$$\Psi(\mathbf{x}_{n+1}) = \mathcal{F}^{-1}\left\{\left[e^{-i\pi\lambda\Delta z(q_x^2+q_y^2)}\right]\mathcal{F}\left[e^{i\sigma\int_z^{z+\Delta z}\mathcal{V}^{\text{int}}(\mathbf{x})\,\mathrm{d}z}\Psi(\mathbf{x}_n)\right]\right\}$$

The propagation of electrons through the whole specimen can then be modelled as consecutive transmission through each slice until the electron wave exits the specimen ($\Psi(\mathbf{x}_{\text{exit}})$). The exit wave is then convoluted by microscope optics (contrast transfer function) and the detector (quantum efficiency, modular transfer function, readout noise, dark current etc..). [13, 14]

### 3.4.1 Molecular model preparation

In order the carry out the multislice simulations, we used molecular dynamics (MD) simulations to prepare input files for the TEMsim software [12]. The program package *moltemplate*, [15] was used to generate input files for the LAMMPS MD software [16]. Each polymer block was separately investigated by using corresponding homopolymer chains in a periodic boundary

1. DIGITALMICROGRAPH version 1.83.842.
2. which does not only depend on electron density $\rho_e$, but also on atomic number $Z$ among other things.

conditions. At the first step only soft potentials and bonded interactions

$$E = A\left[1 + \cos\left(\frac{\pi r}{r_c}\right)\right] + \sum_{\text{bonds}} K_r(r - r_0)^2, \qquad r > r_c$$

were included to allow chains move through each other for fast chain entanglement, while simulation box was slowly squeezed from a initial density $0.1\,\mathrm{g/cm^3}$ to a final volume of $4.49 \times 4.49 \times (5 \cdot 4.49)\,\mathrm{nm^3}$. The number of chains and repeat units, 30–65 and 55–65 respectively, were selected in order to match the final volumes with bulk densities (cf. Table S1) of the respective homopolymers. The consecutive and energy minimization and NVT simulations were carried out using the OPLS-AA force field[17] at 300 K using Nosé-Hoover thermostat. The OPLS-AA force field parameters were consulted from literature [18–23]. All the output files from homopolymer MD simulations where concatenated to one input file for the TEM simulations to ensure consistent intensity scaling for all blocks.

A snapshot from MD and TEM simulations is shown in Fig. S2. It is remarkable that there is no discernible contrast between the different blocks in TEM. Even silicon rich PDMS, perhaps due to its relatively low bulk density, is indistinguishable from the rest of blocks. Therefore we conclude that very little can said about the system from unstained TEM measurements.

### 3.5 Electron tomography data acquirement and analysis

Electron tomographic tilt series were acquired with the SerialEm-software[3] package [24]. Samples were tilted between $\pm 69^\circ$ angles with 2–3° increment step depending on the beam sensitivity of the sample. Alignment of tilt image series was done with Imod software package [25]. Initially we used maximum entropy (MEM) reconstruction scheme using Mem-program on a Linux cluster with regularization parameter $\delta$ value $5.0 \times 10^{-2}$ [26]. Later, we implemented a Total Variation (TV) reconstruction scheme for improved resolution according to Jensen et al[27], and Astra toolbox [28, 29] was used for construction the projection and backprojection operators. For isosurface rendering, reconstructed volumes were segmented using trainable Weka segmentation [30].

3. SerialEm version 3.2.2

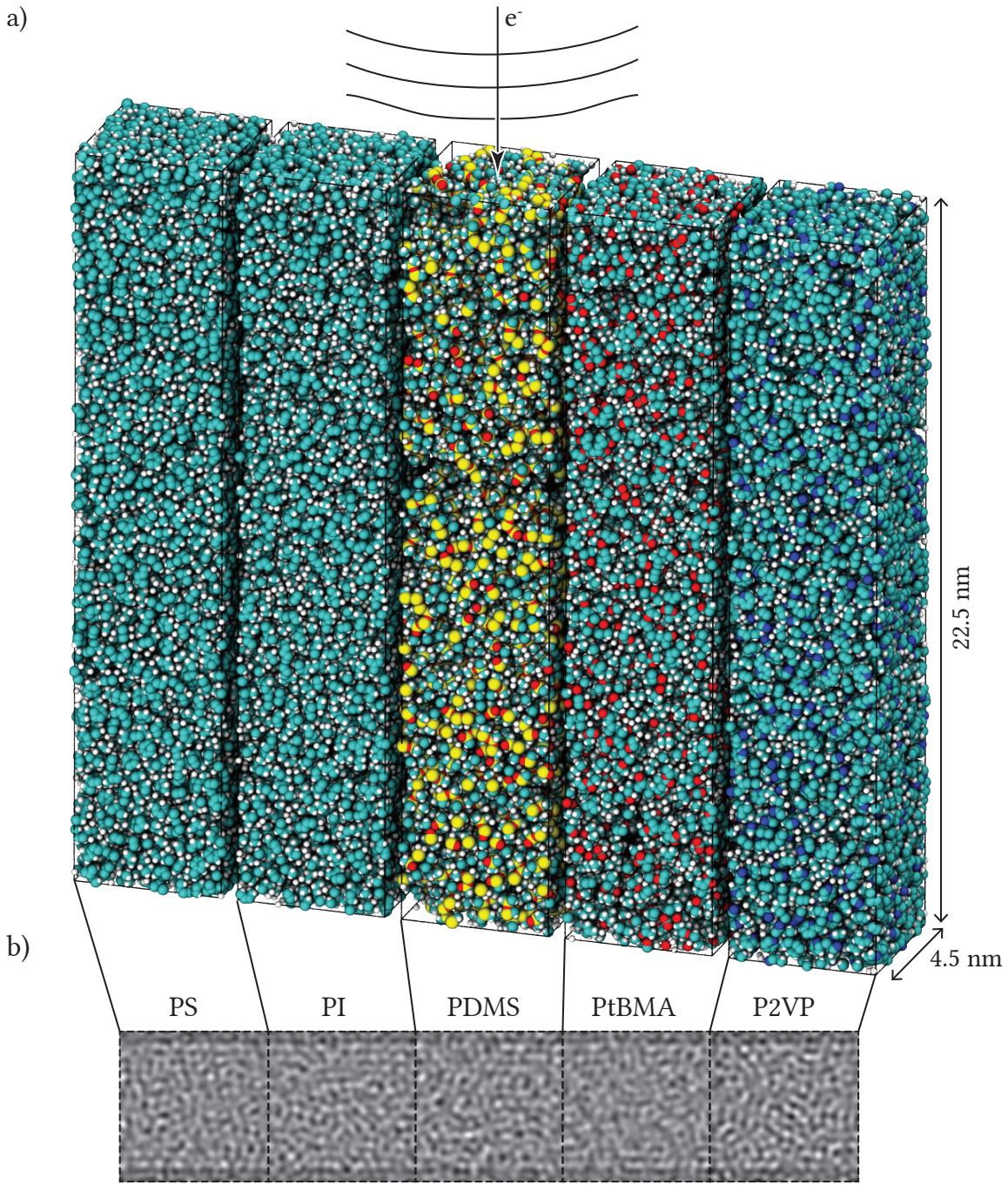


**Fig**. S2: a) Molecular dynamic simulations of different blocks in cuboid volumes and b) simulated TEM images using the multislice method. The simulations indicate that without staining there is no discernible difference in contrast between the blocks in TEM.

# 4 Results

## 4.1 Cryovitrification

In order to exclude drying artifacts, reference TEM micrographs were collected from cryovitrified samples S3

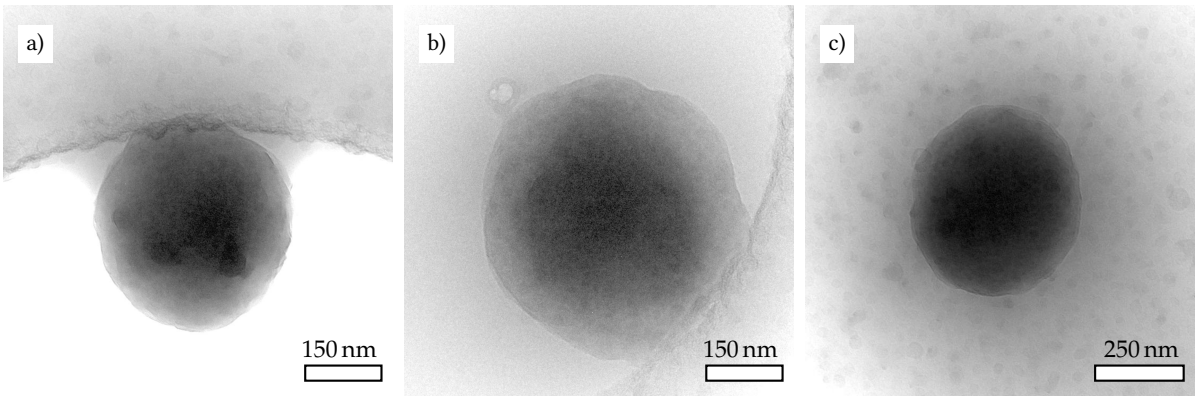


**Fig.** S3: Vitrified polymersomes. a) One suspended by vitrified acetone. b) One partly embedded in a vitrified film, c) and one resting on carbon film. The polymersomes attract a small vitrified region of acetone, which is seen as a gradient around the polymersomes

### 4.2 Stained samples

#### 4.2.1 Iodine staining

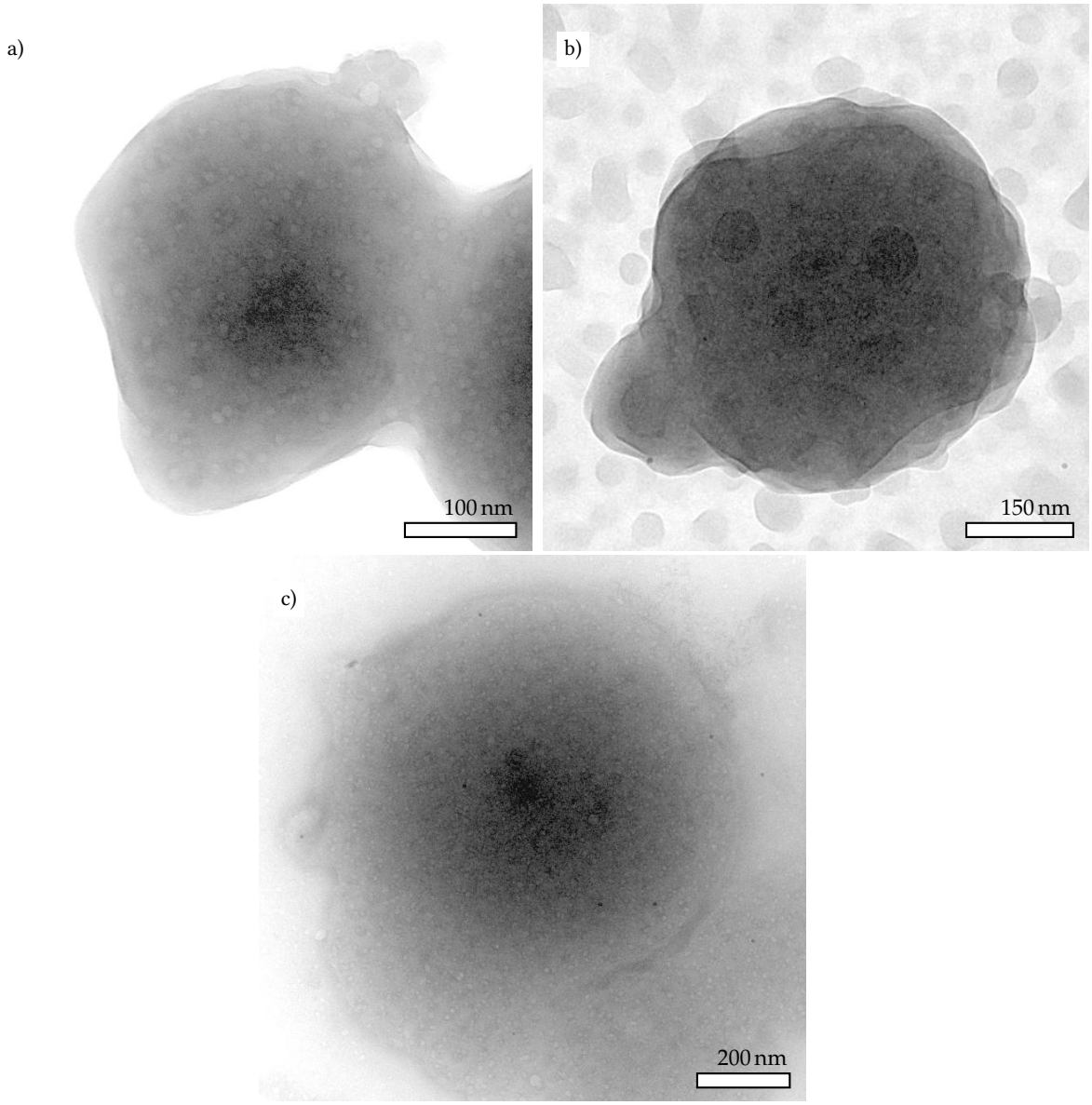


**Fig**. S4: The polymersomes are deformed after $I_2$ staining. This deformation appears to facilitate cavity formation (white spots) inside the polymersomes.

### 4.2.2 $OsO_4$ staining

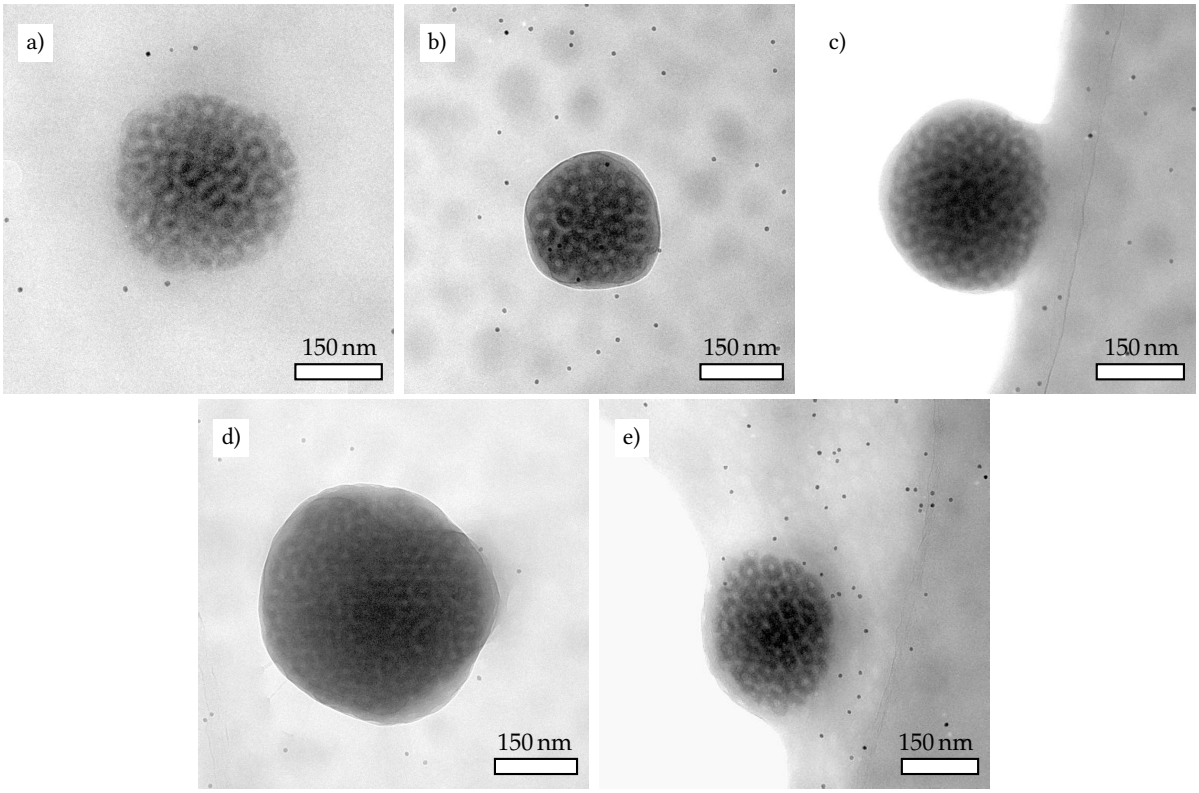


**Fig**. S5: Week old samples drop casted on carbon film and stained with $OsO_4$. The stained PI seems to microphase separate into rings inside the polymersomes. The small black dots ($d \sim 10\,\text{nm}$) are fiducial gold markers used for tomographic purposes.

### 4.2.3 $RuO_4$ staining

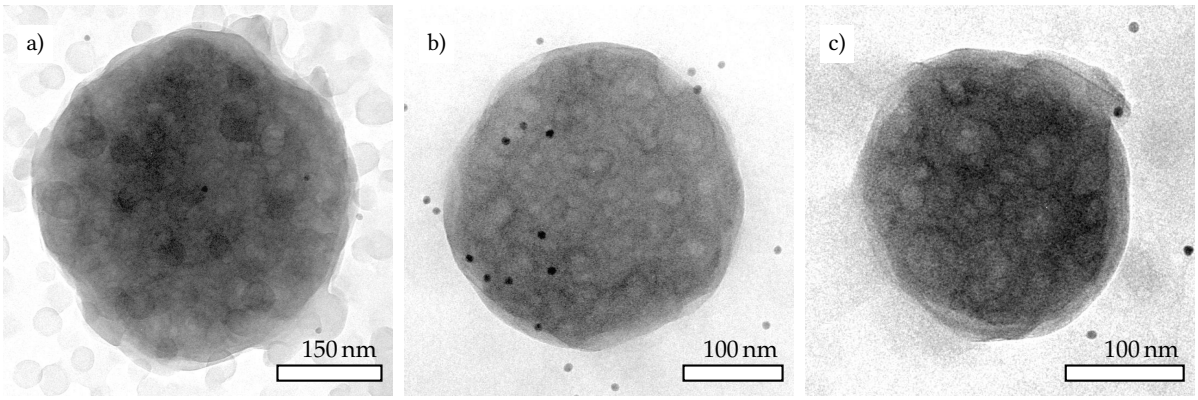


**Fig**. S6: Fresh samples show concentric rings inside polymersomes after drying and $RuO_4$ staining for 5 min.

### 4.3 Electron tomography

For quantitative assessment on microphase separated structures, we calculated radial distribution functions, that is, the observed intensity (transmission) as function of distance from center of core-shell subunits, from several (MEM) reconstructions for each stained sample.

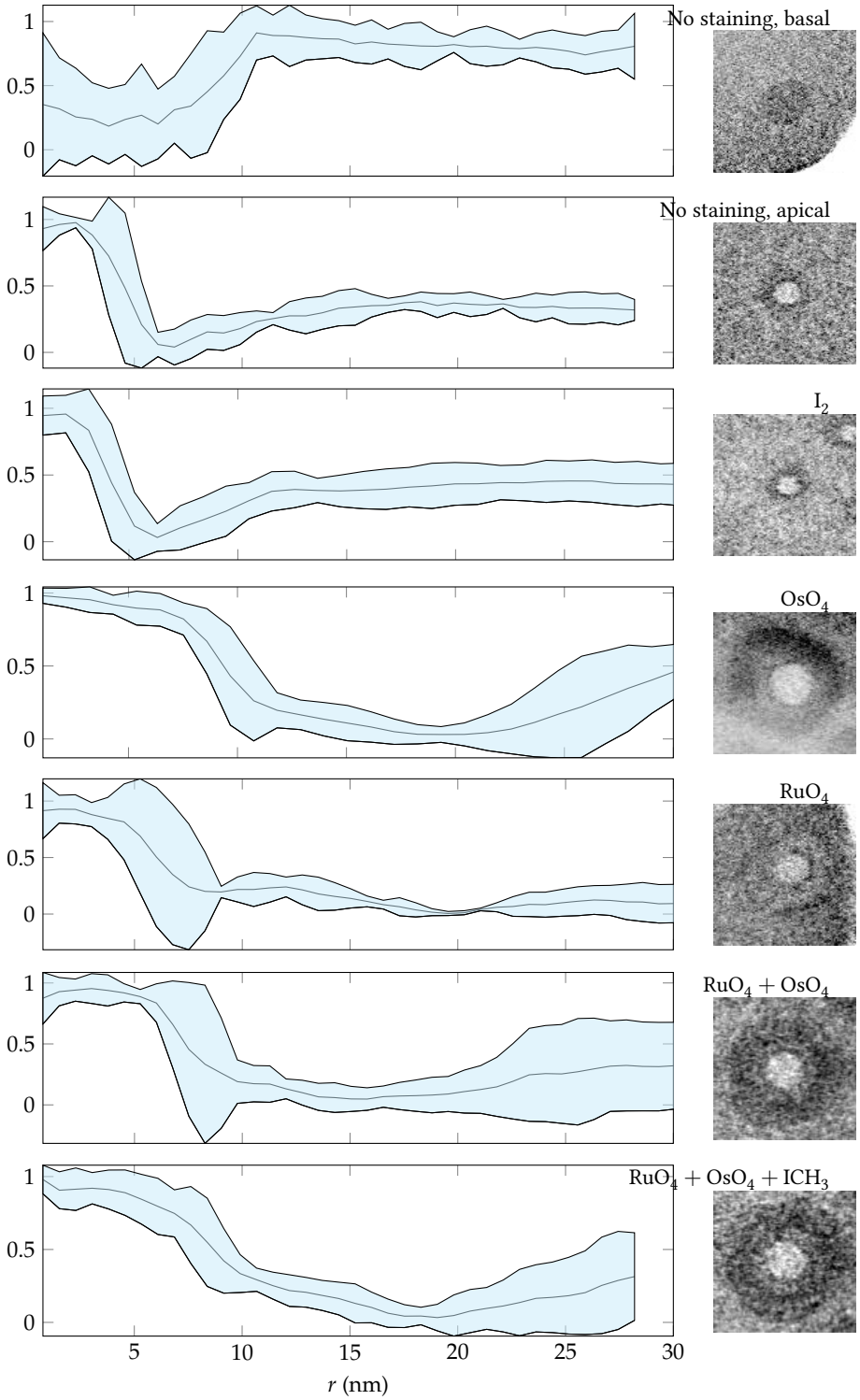


**Fig**. S7: RDFs of subregions of evaporated acetone samples with different staining. Grey, shaded area depicts the 95 % point-wise trust regions. Images on the right show snapshots of subunits from ET reconstruction

### 4.4 Dynamic light scattering

The dynamic light scattering (DLS) measurements were conducted using a Brookhaven Instruments Co. goniometer Bic-200SM, a Bic-TurboCorr digital pseudo-cross-correlator and a Bic-CrossCorr detector combining two Bic-DS1 detectors. Pseudo-cross-correlation functions of the scattered light intensity were collected with the self-beating method [31]. A Sapphire $488-100$ Cdrh laser from Coherent GmbH operating at $\lambda_0 = 488\,\mathrm{nm}$ and power adjusted in the range from 10 and 60 mW was used as a light source. The measurements were performed in cylindrical glass sample cells 11 mm in diameter. The temperature of the samples was controlled by means of a Lauda RC 6C thermostat. All the LS studies were performed at 20 °C. Refractive index values $n_{PS} = 1.5729$ and $n_{\mathrm{Acetone}} = 1.359$ were used for particles and solvent in DLS data analysis respectively

To avoid multiple scattering in DLS, the standard $1\,\%\,(\mathrm{w/w})$ solutions were diluted by a factor of $\times\ 80$ by dissolving 1.97 mg of the block copolymer to 16 mL acetone ($\Rightarrow\ c = 0.12\,\mathrm{g/l} \Leftrightarrow 0.012\,\%\,(\mathrm{w/w})$) that had been filtered through superpure™ PTFE-0.22 µm filter. The sample solution was mixed with an IKA® shaker and was then left to equilibrate for 24 h.

To clean samples from dust contaminants while avoiding filtering larger block copolymer particles, the sample solution was centrifuged for 15 min at 8000 rpm to sediment the dust. The sample solvent was then transferred to a DLS sample cell, which had been cleaned with methanol that was filtered through Millex®-HV hydrophilic PVDF filter.

#### 4.4.1 DLS results

DLS is standard method for evaluating particle size distribution of dilute colloid samples. Most reliable results are obtained when one is characterizing a monodisperse or monomodal samples. However it is possible to obtain missleadingly monomodal or otherwise inaccurate size distribution reconstructions in DLS from samples that are multimodal if necessary care is not taken. To avoid such caveats, we checked the DLS results for our system against 14 detection angles; 30, 35, 40, 45, 50, 60, 70, 80, 90, 110, 120, 135, 140 and 150 since it is know that for multimodal samples DLS results are angle dependent.[32–35] Unfortunately the available DLS setup does not allow multiangle analysis and therefore only separate estimates are given.

The average diameter of the particles was evaluated using the cumulant method [36]. Evidently, the diameter is highly angle dependent, ranging between 150 nm–260 nm (see Table S3), which is typical for polydisperse samples. Contin analysis shows (see Fig. S8) angle dependence to some degree , and the particle size distribution is estimated to be between 100 nm–300 nm. Since the sample is obviously polydisperse and in the other hand extensive multiangle dynamic light scattering analysis is beyond the scope of this article, we take the DLS results to be tentative only as they roughly agree on the size range of the polymersomes observed in TEM.

Table S3: Average hydrodynamic diameters based on cumulant analysis for the particles at $c = 0.12\,\mathrm{g/l}$ at 20 °C at different detection angles.

| $\theta\ [^\circ]$ | $d_H$ [nm] |
|---|---|
| 30 | 258.7 |
| 35 | 254.3 |
| 40 | 253.1 |
| 45 | 199.4 |
| 50 | 188.6 |
| 60 | 168.1 |
| 70 | 160.3 |
| 80 | 150.0 |
| 90 | 140.9 |
| 110 | 134.1 |
| 120 | 135.3 |
| 135 | 135.3 |
| 140 | 138.7 |
| 150 | 146.3 |

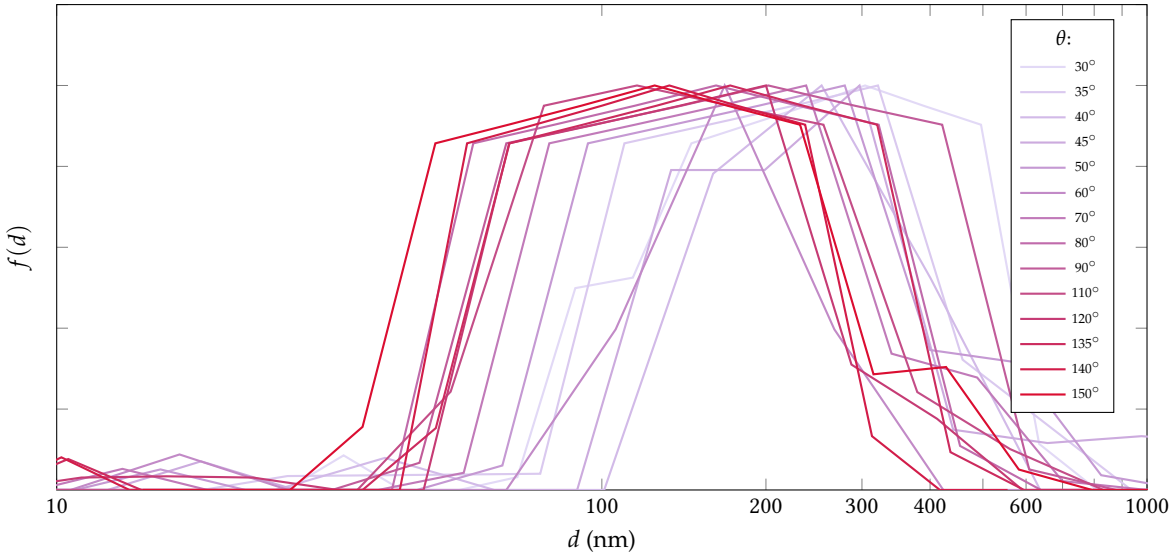


**Fig**. S8: Estimated particle size distribution of PS-*b*-PI-*b*-PDMS-*b*-PtBMA-*b*-P2VP in acetone ($c = 0.12\,\mathrm{g/l}$, 20 °C) using CONTIN analysis. The coarseness of plots is due to the fact that the CONTIN method automatically reduces the resolution to obtain better fits.

## References


[1] P. Fragouli, H. Iatrou, D. J. Lohse, and N. Hadjichristidis. Linear pentablock quintopolymers (l-SIDMV) with five incompatible blocks: Polystyrene, polyisoprene-1,4, poly(dimethylsiloxane), poly(*tert*-butyl methacrylate), and poly-(2-vinylpyridine). *Journal of Polymer Science Part A: Polymer Chemistry*. **2008**, *46*, 12, pp. 3938–3946. ISSN: 1099-0518. DOI: 10.1002/pola.22732.

[2] D. W. van Krevelen. *Properties of Polymers, Their Correlation with Chemical Structure; their Numerical Estimation and Prediction from Additive Group Contributions*. Ed. by K. te Nijenhuis. 4th Edition. Elsevier Science, 2009. ISBN: 9780080548197. URL: http://store.elsevier.com/Properties-of-Polymers/D_W_-van-Krevelen/isbn-9780080548197/.

[3] J. E. Mark. *Physical properties of polymers handbook*. Springer, 2007. ISBN: 9780387312354. URL: http://www.springer.com/chemistry/polymer+science/book/978-0-387-31235-4.

[4] E. Dalal, K. Taylor, and P. Phillips. The equilibrium melting temperature of cis-polyisoprene. *Polymer*. **1983**, *24*, 12, pp. 1623–1630. ISSN: 0032-3861. DOI: http://dx.doi.org/10.1016/0032-3861(83)90182-9.

[5] A. Takano, K. Soga, T. Asari, J. Suzuki, S. Arai, H. Saka, and Y. Matsushita. Observation of Four-Phase Lamellar Structure from a Tetrablock Quarterpolymer of the ABCD Type. *Macromolecules*. **2003**, *36*, 22, pp. 8216–8218. DOI: 10.1021/ma034981m.

[6] T. Matsuyama and Y. Kawata. Effects of Solvent and Ambient Humidity on Nanodot Structures for Near-Field Optical Data Storage Using Self-Assembled Diblock Copolymer. *Japanese Journal of Applied Physics*. **2005**, *44*, 5S, p. 3524. URL: http://stacks.iop.org/1347-4065/44/i=5S/a=3524.

[7] S. A. B. Shamsudin, G. Sakaguchi, M. Takenaka, and H. Hasegawa. Influence of Temperature and Type of Solvents on the Microdomain Orientation of PS-b-P2VP Ultrathin Films by Solvent Annealing. *Macromolecular Symposia*. **2013**, *327*, 1, pp. 72–79. ISSN: 1521-3900. DOI: 10.1002/masy.201350508.

[8] H. Fan and Z. Jin. Freezing polystyrene-b-poly(2-vinylpyridine) micelle nanoparticles with different nanostructures and sizes. *Soft Matter*. **2014**, *10*, pp. 2848–2855. DOI: 10.1039/C3SM53049C.

[9] J. Raula, J. Shan, M. Nuopponen, A. Niskanen, H. Jiang, E. I. Kauppinen, and H. Tenhu. Synthesis of Gold Nanoparticles Grafted with a Thermoresponsive Polymer by Surface-Induced Reversible-Addition-Fragmentation Chain-Transfer Polymerization. *Langmuir*. **2003**, *19*, 8, pp. 3499–3504. DOI: 10.1021/la026872r.

[10] F. Schacher, A. Walther, M. Ruppel, M. Drechsler, and A. H. E. Müller. Multicompartment Core Micelles of Triblock Terpolymers in Organic Media. *Macromolecules*. **2009**, *42*, 10, pp. 3540–3548. DOI: 10.1021/ma9002424.

[11] K. Takahashi, H. Hasegawa, T. Hashimoto, V. Bellas, H. Iatrou, and N. Hadjichristidis. Four-Phase Triple Coaxial Cylindrical Microdomain Morphology in a Linear Tetrablock Quaterpolymer of Styrene, Isoprene, Dimethylsiloxane, and 2-Vinylpyridine. *Macromolecules*. **2002**, *35*, 13, pp. 4859–4861. DOI: 10.1021/ma0255074.

[12] E. J. Kirkland. *Advanced Computing in Electron Microscopy*. Springer US, 2010. DOI: 10.1007/978-1-4419-6533-2.

[13] M. Vulović, R. B. Ravelli, L. J. van Vliet, A. J. Koster, I. Lazić, U. Lücken, H. Rullgård, O. Öktem, and B. Rieger. Image formation modeling in cryo-electron microscopy. *Journal of Structural Biology*. **2013**, *183*, 1, pp. 19–32. DOI: 10.1016/j.jsb.2013.05.008.

[14] I. Lobato, S. V. Aert, and J. Verbeeck. Progress and new advances in simulating electron microscopy datasets using {MULTEM}. *Ultramicroscopy*. **2016**, *168*, pp. 17–27. ISSN: 0304-3991. DOI: http://dx.doi.org/10.1016/j.ultramic.2016.06.003.

[15] A. Jewett. Moltemplate (manuscript in preparation). **2017**. URL: http://www.moltemplate.org/.

[16] S. Plimpton. Fast Parallel Algorithms for Short-Range Molecular Dynamics. *Journal of Computational Physics*. **1995**, *117*, 1, pp. 1–19. ISSN: 0021-9991. DOI: http://dx.doi.org/10.1006/jcph.1995.1039.

[17] W. L. Jorgensen and J. Tirado-Rives. The OPLS [optimized potentials for liquid simulations] potential functions for proteins, energy minimizations for crystals of cyclic peptides and crambin. *Journal of the American Chemical Society*. **1988**, *110*, 6, pp. 1657–1666. DOI: 10.1021/ja00214a001.

[18] R. M. Sok. Permeation of small molecules across a polymer membrane: a computer simulation study. PhD thesis. **1994**.

[19] R. Faller, F. Müller-Plathe, M. Doxastakis, and D. Theodorou. Local Structure and Dynamics of trans-Polyisoprene Oligomers. *Macromolecules*. **2001**, *34*, 5, pp. 1436–1448. DOI: 10.1021/ma0016782.

[20] J. S. Smith, O. Borodin, and G. D. Smith. A Quantum Chemistry Based Force Field for Poly(dimethylsiloxane). *The Journal of Physical Chemistry B*. **2004**, *108*, 52, pp. 20340–20350. DOI: 10.1021/jp047434r.

[21] V. A. Harmandaris, N. P. Adhikari, N. F. A. van der Vegt, and K. Kremer. Hierarchical Modeling of Polystyrene: From Atomistic to Coarse-Grained Simulations. *Macromolecules*. **2006**, *39*, 19, pp. 6708–6719. DOI: 10.1021/ma0606399.

[22] Z. A. Makrodimitri, R. Dohrn, and I. G. Economou. Atomistic Simulation of Poly(dimethylsiloxane):Force Field Development, Structure, and Thermodynamic Properties of Polymer Melt and Solubility of n-Alkanes, n-Perfluoroalkanes, and Noble and Light Gases. *Macromolecules*. **2007**, *40*, 5, pp. 1720–1729. DOI: 10.1021/ma062453f.

[23] T. V. M. Ndoro. Simulation of a Polystyrene Silica Nanocomposite. PhD thesis. Technischen Universität Darmstadt, **2011**. URL: http://tuprints.ulb.tu-darmstadt.de/2830/1/Ndoro_Tinashe_-_Thesis_2011.pdf.

[24] D. N. Mastronarde. Automated electron microscope tomography using robust prediction of specimen movements. *Journal of Structural Biology*. **2005**, *152*, 1, pp. 36–51. ISSN: 1047-8477. DOI: 10.1016/j.jsb.2005.07.007.

[25] J. R. Kremer, D. N. Mastronarde, J. R. McIntosh, et al. Computer visualization of three-dimensional image data using IMOD. *Journal of structural biology*. **1996**, *116*, 1, pp. 71–76. URL: http://bio3d.colorado.edu/imod/paper/.

[26] P. Engelhardt. Electron Tomography of Chromosome Structure. In: *Encyclopedia of Analytical Chemistry*. John Wiley & Sons, Ltd, **2006**. ISBN: 9780470027318. DOI: 10.1002/9780470027318.a1405.

[27] T. L. Jensen, J. H. Jørgensen, P. C. Hansen, and S. H. Jensen. Implementation of an optimal first-order method for strongly convex total variation regularization. *BIT Numerical Mathematics*. **Jan. 2011**, *52*, 2, pp. 329–356. DOI: 10.1007/s10543-011-0359-8.

[28] W. Palenstijn, K. Batenburg, and J. Sijbers. Performance improvements for iterative electron tomography reconstruction using graphics processing units (GPUs). *Journal of Structural Biology*. **2011**, *176*, 2, pp. 250–253. ISSN: 1047-8477. DOI: http://dx.doi.org/10.1016/j.jsb.2011.07.017.

[29] W. van Aarle, W. J. Palenstijn, J. D. Beenhouwer, T. Altantzis, S. Bals, K. J. Batenburg, and J. Sijbers. The ASTRA Toolbox: A platform for advanced algorithm development in electron tomography. *Ultramicroscopy*. **2015**, *157*, pp. 35–47. ISSN: 0304-3991. DOI: http://dx.doi.org/10.1016/j.ultramic.2015.05.002.

[30] M. Hall, E. Frank, G. Holmes, B. Pfahringer, P. Reutemann, and I. H. Witten. The WEKA Data Mining Software: An Update. *SIGKDD Explorations*. **2009**, *11*, 1. URL: http://kdd.org/Explorations/view/july-2009-volume-11-issue-1.

[31] B. Chu. *Laser Light Scattering: basic princibles and practice*. Academic Press (CA), 1991. ISBN: 0121745511.

[32] R. Buttgereit, M. Marth, and J. Honerkamp. Estimation of distribution functions in light scattering: the regularization method and Bayes' Ansatz. *Macromolecular Symposia*. **2000**, *162*, 1, pp. 149–172. DOI: 10.1002/1521-3900(200012)162:1<149::AID-MASY149>3.0.CO;2-M.

[33] J. R. Vega, L. M. Gugliotta, V. D. Gonzalez, and G. R. Meira. Latex particle size distribution by dynamic light scattering: novel data processing for multiangle measurements. *Journal of Colloid and Interface Science*. **2003**, *261*, 1, pp. 74–81. ISSN: 0021-9797. DOI: 10.1016/S0021-9797(03)00040-7.

[34] L. A. Clementi, J. R. Vega, L. M. Gugliotta, and H. R. Orlande. A Bayesian inversion method for estimating the particle size distribution of latexes from multiangle dynamic light scattering measurements. *Chemometrics and Intelligent Laboratory Systems*. **2011**, *107*, 1, pp. 165–173. ISSN: 0169-7439. DOI: 10.1016/j.chemolab.2011.03.003.

[35] L. A. Clementi, J. R. Vega, H. R. Orlande, and L. M. Gugliotta. Size distribution of nanoparticles by dynamic light scattering. Comparison of Bayesian and Tikhonov inversion methods. *Inverse Problems in Science and Engineering*. **2012**, *20*, 7, pp. 973–990. DOI: 10.1080/17415977.2012.658518.

[36] D. E. Koppel. Analysis of Macromolecular Polydispersity in Intensity Correlation Spectroscopy: The Method of Cumulants. *The Journal of Chemical Physics*. **1972**, *57*, 11, pp. 4814–4820. DOI: http://dx.doi.org/10.1063/1.1678153.